

Available online at www.sciencedirect.com

ScienceDirect

www.elsevier.com/locate/jes

JES
 JOURNAL OF
 ENVIRONMENTAL
 SCIENCES
www.jesc.ac.cn

Uranium speciation in coal bottom ash investigated via X-ray absorption fine structure and X-ray photoelectron spectra

Yinglong Sun^{1,2}, Menxin Wu¹, Lirong Zheng³, Bangda Wang², Yi Wang^{2,*}

1. National Meteorological Center, China Meteorological Administration, Beijing 100081, China

2. Key Laboratory for Solid Waste Management and Environment Safety, Ministry of Education of China, Tsinghua University, Beijing 100084, China

3. Beijing Synchrotron Radiation Facility, Institute of High Energy Physics, Chinese Academy of Sciences, Beijing 100039, China

ARTICLE INFO

Article history:

Received 6 December 2017

Revised 13 February 2018

Accepted 14 February 2018

Available online 27 February 2018

Keywords:

Coal bottom ash

Uranium speciation

XAFS

Uranium migration

ABSTRACT

Similar to chromium contamination, the environmental contamination caused by uranium in radioactive coal bottom ash (CBA) is primarily dependent on the chemical speciation of uranium. However, the relationship between uranium speciation and environmental contamination has not been adequately studied. To determine the relationship between uranium speciation and environmental contamination, X-ray absorption fine structure (XAFS) and X-ray photoelectron spectra (XPS) analyses were performed to determine the uranium speciation in CBA exposed to different chemical environments and simulated natural environments. The leachability of the different forms of uranium in the CBA was studied via a simulated acid rain leaching experiment, and the results showed that 57.0% of the total uranium was leached out as U(VI). The results of a linear combination fit (LCF) of the X-ray absorption near edge structure (XANES) spectrum revealed that in the raw CBA, the uranium mainly occurred as U_3O_8 (71.8%). However, in the iron-rich particles, the uranium mainly occurred as UO_2 (91.9%) after magnetic separation. Magnetite is a ubiquitous ferrous-bearing oxide, and it was effective for the sorption of U(IV). The result of $FeSO_4$ leaching experiment indicated that 96.57% of total uranium was reduced from U(VI) to U(IV) when infiltrated with the $FeSO_4$ solution for 6 months. This result clearly demonstrated the changes in chemical valence of uranium in the coal ash and provided a conceptual principle for preventing uranium migration from ash to the surrounding soil and plants.

© 2017 The Research Center for Eco-Environmental Sciences, Chinese Academy of Sciences.

Published by Elsevier B.V.

Introduction

Lignite is a type of coal with incomplete coalification, and varieties of lignite produced in several locations around the world, including South Texas (USA) (Mohan et al., 1982), Ajka Valley (Hungary) (Papp et al., 2002), Figueira County (Brazil) (Flues et al., 2006), the southern Urals and Transbaikalia (Russia) (Seredin and Finkelman, 2008), and northern Greece, are highly enriched in U (Yang, 2007). Middle Asia may represent the area with the most abundant uranium-bearing lignite (Seredin

and Finkelman, 2008). However, few studies have focused on the chemical speciation of uranium. The oxidation state was a fundamental property of uranium speciation and the key factor responsible for uranium's solubility and mobility (Bertsch et al., 1994). Uranium in the environment usually occurs in two redox states: U(VI) and U(IV) (Singer et al., 2012). Hexavalent uranium ($U(VI)O_2^{2+}$) is soluble and easily forms U(VI) complexes with various ligands, such as carbonates in groundwater (Gui et al., 2009), which increases the solubility of uranium by several orders of magnitude (Dong and Brooks, 2006; Stewart et al., 2010).

* Corresponding author. E-mail: yi_wang@tsinghua.edu.cn (Yi Wang).

However, tetravalent uranium U(IV) is often immobilized as solid U(IV) compounds, such as uraninite (UO₂), which inhibits the transport of uranium between contaminated soils and groundwater (Langmuir, 1978; Mei et al., 2015).

X-ray absorption fine structure (XAFS) is an ideal tool for detecting the local chemical environment and structures of heavy metals in complex solid samples, and it does not alter the sample status (Mansour and Melendres, 1998; Hsiao et al., 2001). X-ray absorption near edge structure (XANES) is a reliable spectroscopic method that has been used to analyze the heavy metal structures in minerals and oxides as well as the structure of metal sorption complexes (Allen et al., 1996; Henning et al., 2002; Wu et al., 1997, 2001, 2004). XANES has also been used to quantitatively analyze the main component concentrations via a linear combination fit (LCF) analysis (Takaoka et al., 2005; Hsiao et al., 2006). In addition, X-ray photoelectron spectroscopy (XPS) is a surface-sensitive technique used to determine the different redox states of uranium surface species, and it has been used to investigate the structural properties (e.g., chemical states, compositions and element distributions) of uranium and variations in its chemical states during reactions. However, in previous studies, the samples included synthetic complexes that presented high concentrations of uranium and were relatively easy to detect. In this work, XPS was used to determine the U(VI) and U(IV) states in coal bottom ash (CBA). Here, XPS and XAFS were used to ascertain the redox state of uranium in CBA.

Previous studies have determined the mode of occurrence of selected trace elements in coal and ash via XAFS spectroscopy. However, few studies have focused on the uranium speciation in ash. Huggins described the different oxidation states of Cl, Ti, V, Cr, Mn, Ni, Zn, and As in coal and combustion ash by XAFS and emphasized different modes of occurrence of arsenic (as arsenic and arsenate) in coal (Huggins and Huffman, 1996; Huggins et al., 2000); however, they did not address the chemical properties of uranium.

In this article, the objectives were to (1) study the leachability of uranium in an ash heap via experimentally simulated acid rain; (2) determine the oxidation condition and uranium electronic structure in CBA by applying XAFS and XPS; and (3) verify our hypothesis that uranium is immobilized in CBA by reducing U(VI) to U(IV) via the addition of a diluted FeSO₄ solution to the CBA heap.

1. Materials and methods

1.1. Samples and reagents

The CBA samples were obtained from two different high-uranium coals in the ash heap in Yunnan Province, China. The samples were crushed with a ball mill and passed through a 500-mesh standard sieve (<25 μm in diameter). The fine powder samples were dried at 105°C in a forced air oven to a constant weight and stored in a desiccator for future use. The CBA was characterized as a uranium-rich (374 mg/kg) material with low-level radioactivity (gross α of 3.08 Bq/g and gross β of 11.83 Bq/g). The two samples did not show significant differences in their components and characteristics; therefore, they were combined together for further investigation.

1.2. CBA column leaching experiment with simulated acid rain

To investigate the leaching of uranium from CBA over long-term periods, the CBA samples were artificially leached with simulated acid rain. The pH of the acid rain ranged from 2 to 4 in the sampling area (Zhang et al., 2007; Yang et al., 2014). Therefore, a synthetic acid rain with pH = 3.0 was prepared with a 3:1 (V/V) H₂SO₄-HNO₃ solution mixture. For the leaching experiment, 25.0 g of CBA was placed in a Plexiglas column (locally fabricated) with an interior diameter of 2 cm and length of 35 cm. The height of the CBA columns in the Plexiglas tubes were approximately 15 cm, and the typical volume was 47 cm³ (Fig. 1). The simulated acid rain was pumped by a peristaltic pump to percolate through the CBA columns at a flow rate of 3 mL/hr. The CBA were exposed to the acid rain for 180 consecutive days. The leachates were collected to determine the uranium concentrations. In the leachate, U(VI) could be directly extracted by Tributyl phosphate (TBP), whereas U(IV) could not be directly extracted. As the TBP had high adsorption on uranyl ion, and no adsorption on U(IV). The uranium content in the leachates was determined by an inductively coupled plasma mass spectrometer (ICP-MS) (Xseries2, Thermo Scientific Company, USA) after extracted by TBP.

1.3. Magnetic separation of the CBA

A total of 20 g of unaltered CBA was added to 2.0 L of distilled water, and the slurry was stirred vigorously with a magnetic rod (3000 gauss) (iron rich 1). This separation was conducted under abiotic and oxic conditions. This procedure was repeated until none of the magnetic fraction was adhered on the magnet, no more magnetic particles was adhered to magnetic rod, the adhered particles could be crushed into beaker with distilled water after adhered on the magnet. Then, the residual parts were further subjected to a wet-type, higher-intensity magnetic

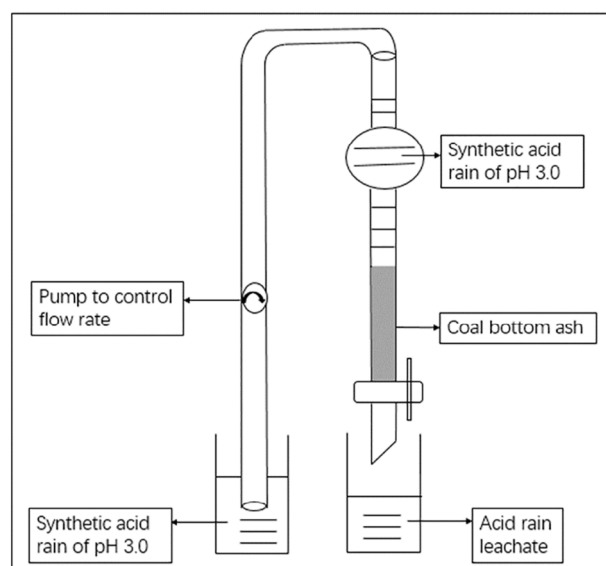


Fig. 1 – Simple equipment diagram showing the simulated acid rain experiment.

separator (XCSQ-50*70, Wuhan Exploring Machinery Factory, China) with a magnetic field intensity of 15,000 gauss (iron rich 2) to collect the weak magnetic fractions. The weak magnetic fraction, strong magnetic fraction, and non-magnetic fraction were oven dried to a constant weight, and their masses were recorded.

1.4. Reduction of uranium by FeSO₄ solution

To reduce the migration of uranium in the CBA, FeSO₄ solution was added as a reductive reagent to the bottom ash heap. A diluted FeSO₄ solution (20 g/L) was sprayed on the bottom ash heap (approximately 300 kg of CBA) three times at an interval of two months between successive sprays to provide sufficient time for the ferrous sulfate solution to infiltrate the entire heap. Uranium concentration in the leachate and leached residue were determined by an inductively coupled plasma mass spectrometer (ICP-MS).

1.5. XAFS and XPS analysis

Uranium LIII-edge XANES samples were obtained at the 1W1B beamline at the Beijing Synchrotron Radiation Facility (BSRF). The spectra of crystalline UO₂(s), UO₃(s), U₃O₈(s) and UO₂(NO₃)₂(s) samples were recorded in transmission mode, whereas the other sample data were collected in fluorescence mode because of the low uranium concentration. The CBA samples were pressed into pieces and fixed onto the sampling channel. The typical energy of the storage ring was 2.5 GeV, and the average current was 200 mA. The absolute energy position was calibrated using a Y metal foil and a Si(111) double-crystal monochromator (Beijing Synchrotron Radiation Facility, Beijing, China). The measured data from XANES were fitted for the analysis by using the IFFEFIT software package (Newville, 2001).

XPS was conducted using an ESCALAB 250Xi photoelectron spectrometer (Thermo Fisher Scientific, USA). Al Ka (1486.6 eV) was the X-ray source set at 200 W, and a pass energy of 50 eV was used for the high-resolution scan.

The data was processed and the use of the correlation between half-step energy and oxidation state was calculated in Origin9.

2. Results and discussion

2.1. U leaching in simulated acid rain

Analogous to most coal combustion ashes, the major components of the CBA samples were SiO₂ and Al₂O₃, which accounted for 83–84 weight percent (wt.%) of the total mass (Table 1). This result was determined by X-Ray Fluorescence (XRF). From the X-ray diffraction (XRD) pattern of the CBA provided in Fig. 2, it can be seen that the solid particles were composed mainly of amorphous aluminosilicate glass and crystalline phases including quartz, mullite, K-feldspar, and a trace amount of cristobalite.

Raw CBA was leached by the simulated acid rain solution (pH = 3), and the uranium concentration in the leachate was detected. 57% of the total uranium was leached out and

Table 1 – Elemental abundances in CBA from Lincang, Yunnan Province, China (oxides of major elements in wt.%).

Elements	Sample No.1	Sample No.2
SiO ₂	65.7	64.1
Al ₂ O ₃	18.6	19.2
CaO	6.92	6.83
LOI	4.11	5.24
Fe ₂ O ₃	4.35	5.33
K ₂ O	2.38	2.54
MgO	0.88	0.99
TiO ₂	0.34	0.54
Na ₂ O	0.17	0.21
MnO	0.10	0.20
WO ₃	0.065	0.074
BaO	0.09	0.08
P ₂ O ₅	0.096	0.055
U ₃ O ₈	0.04	0.04
SrO	0.04	0.08
Rb ₂ O	0.031	0.054
Cr ₂ O ₃	0.034	0.076
ZrO ₂	0.026	0.063
GeO ₂	0.027	0.042
ZnO	0.021	0.030
NbO	0.017	0.013
NiO	0.016	0.017

CBA: coal bottom ash.

occurred as U(VI), and 41.6% (as U(IV)) remained in the CBA. This result indicated that the leaching of uranium from the CBA was primarily dependent on the uranium chemical state. U(VI) is soluble and can be leached as a uranyl ion, whereas U(IV) is insoluble and can be immobilized. Therefore, the transformation from the soluble U(VI) to the insoluble U(IV) can immobilize uranium and reduce uranium immigration, thereby reducing uranium pollution.

2.2. XPS and XANES studies of uranium in CBA

The XPS spectrum for uranium was recorded in the raw CBA to identify the uranium oxidation state. XPS is capable of

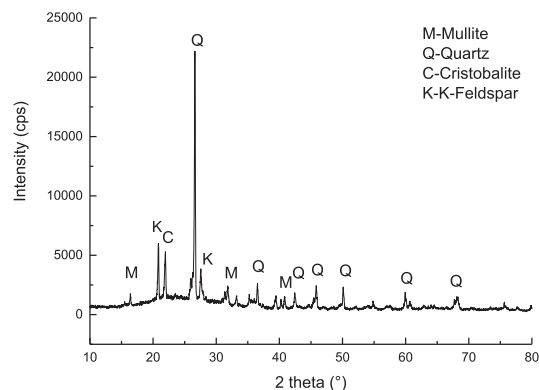


Fig. 2 – XRD patterns of coal bottom ash samples. The X-ray diffraction (XRD) analysis of samples was carried out on a D8 Advance X-ray diffractometer with Cu K α radiation. Scans were done at 40 kV and 40 mA, from 2 θ = 10° to 90°, with the increment of 0.02°.

discerning different oxidation states (Vanden et al., 2000), and XPS spectra are usually sensitive to the oxidation states of ions and their chemical bonding environment in the structure of subjects (Zhang et al., 2014).

The peaks in Fig. 3 show the presence of two different chemical environments. The spectrum was divided into two components, and $U4f_{7/2}$ peak and $U4f_{5/2}$ peak were identified. The $U4f_{7/2}$ and $U4f_{5/2}$ peaks were located at 381.87 eV and 392.87 eV, respectively. The $U4f_{7/2}$ peak of the raw CBA was positioned at 381.87 eV, which was close to the $U4f_{7/2}$ line of UO_3 (382 eV). The $U4f_{7/2}$ peak of U_3O_8 (381.5 eV) (Table 2) generally corresponded to the hexavalent state of uranium. The $U4f_{5/2}$ peak was located at 392.87 eV between the $U4f_{5/2}$ line of UO_3 (393.0 eV) and the $U4f_{5/2}$ peak of U_3O_8 (392.4 eV) (Strehle, 2011), which likely indicated that the binding of uranium occurred as U(VI) in the oxidation state. Thus, these results clearly indicate that the uranium in the CBA mainly occurred as a mixed valence compound of U_3O_8 and UO_3 .

The uranium in the raw CBA was a mixed valence compound in which the metal occurred in two formal oxidation states. Fig. 3 shows that the two fitting peak positions of $U4f_{7/2}$ and $U4f_{5/2}$ were equivalent to UO_3 and U_3O_8 , respectively, which suggests that the two components were mainly UO_3 and U_3O_8 . These results were consistent with findings of the XAFS studies.

The XANES results of the raw ash, iron-rich particles and acid-leached residue are shown in Figs. 4 and 5. By using the energy of the absorption edge at the half-height of the normalized XANES for U(4+), U(5.25+), and U(6+) as reference materials, a high linear correlation ($R^2 = 0.9987$) of the edge energy to the oxidation state was obtained. The correlation of the half-step energy of the U LIII edge and the uranium valence state are shown in Fig. 5.

Fig. 5 indicates that the chemical valences of uranium in the iron-rich particles 1 and 2 and acid-leached residue were +4.40, +4.44 and +4.82, respectively, whereas that of raw ash was +5.33. The valence of uranium in the raw ash was the highest, whereas the valence of uranium in the iron-rich particles was the lowest. These results show that the average valence decreased with the iron-rich particles, indicating a concentration of U(IV) in iron-rich particles, which were then separated out by magnetic separation.

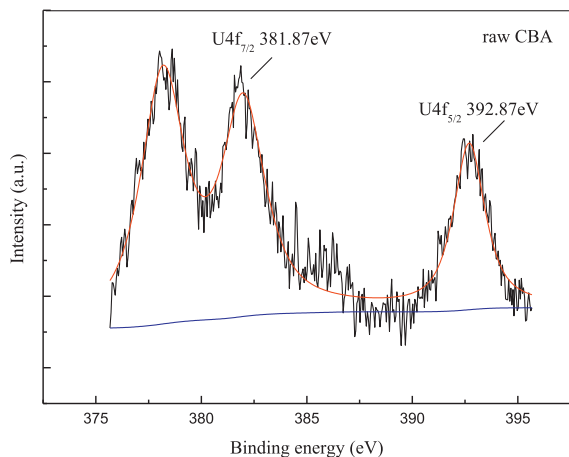


Fig. 3 – X-ray photoelectron spectra (XPS) of raw coal bottom ash (CBA) shows the different peak positions of U.

Table 2 – XPS parameters of standard uranium oxides and raw CBA sample.

	U 4f _{7/2} (eV)	U 4f _{5/2} (eV)	References
CBA sample	381.87	392.87	In this study
UO ₂ main peaks	379.2–380.9	390.0–391.8	Strehle, 2011
U ₃ O ₈ main peaks	381.5	392.4	Strehle, 2011
UO ₃ main peaks	382.0	393.0	Wang et al., 1997

The XPS spectra showed that the CBA was composed of two major species of uranium-containing oxides. The linear combination LCF was performed on k3-weighted XANES spectra to confirm these structures and determine these complex proportions. The LCF results further verified the valence variations after magnetic separation. The LCF of the U L-edge XANES spectrum was successfully used to determine the uranium species in the CBA and iron-rich CBA particles. The spectra of UO_2 , U_3O_8 , and UO_3 were referred to as reference compounds (Table 3). A lower R factor induced a better fit (Laurette et al., 2012). The confidence interval in the percentage is 10%.

The LCF results indicated that in the raw CBA, 71.8% of the total uranium presented as U_3O_8 , 18.7% presented as UO_2 and 12.1% presented as UO_3 . However, in the iron-rich particles, UO_2 accounted for more than 90% of the total uranium, which indicated that U(VI) was largely reduced to U(IV) in the iron-rich particles. The linear-combination analysis of the XANES spectrum revealed that the majority of U(VI) reduced to U(IV), which was determined via magnetic separation.

The simulated acid-leached residue also showed that the valence of uranium decreased compared with that of raw CBA. The U(VI) in raw CBA occurred as UO_3 and part of U_3O_8 , and it was leached out in the acid leaching experiment. U(IV) is insoluble, and in the residue, it mainly occurred as UO_2 .

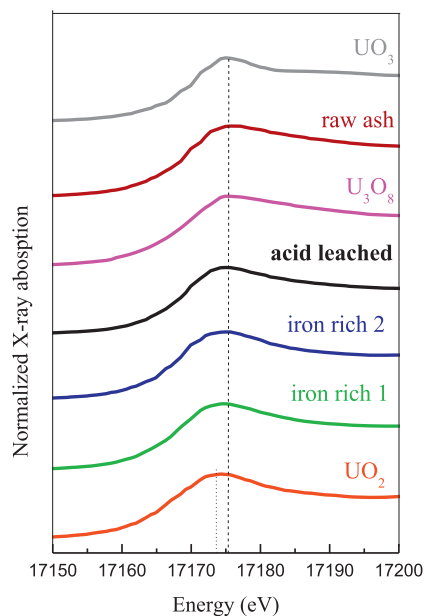


Fig. 4 – X-ray absorption near edge structure (XANES) spectra of standard U(VI), U(IV), and U_3O_8 samples and different CBA samples.

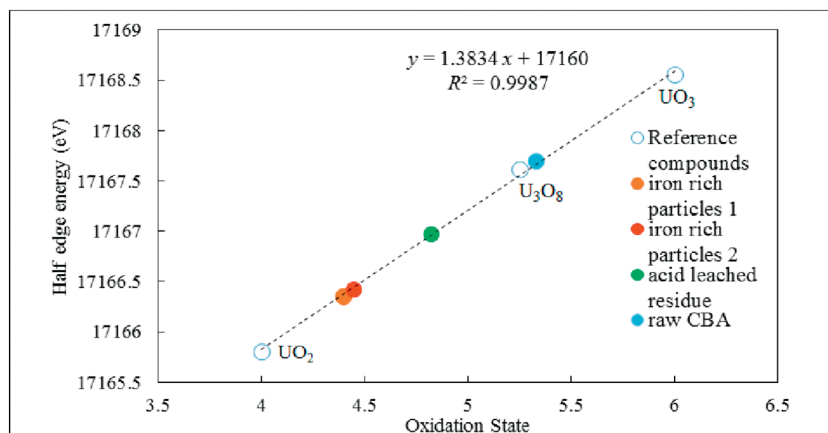


Fig. 5 – Correlation of the half step energy of the uranium LIII-edge with the oxidation states of different species.

This result corresponded with previous studies, which showed that U(VI) had much higher solubility than U(IV).

2.3. Explanation of valance changes during magnetic separation

The iron-rich bottom ash (mainly magnetite) concentrated abundant U(IV) on the surface of the ash particles under abiotic and oxic conditions. The presence of Fe^{2+} in magnetite could reduce U(VI) to U(IV) under abiotic and oxic conditions, which was explained by XAFS.

The relationship between uranium and magnetite has been studied in recent decades. Grambow et al. (1996) studied the sorption of U(VI) onto canister corrosion products, including magnetite, and observed that U(VI) was reduced to U(IV). Recently, Dodge et al. (2002) investigated the association of uranium with various iron oxides, including magnetite, which are commonly formed on corroded steel surfaces. Their study focused on the incorporation of uranium during iron oxide precipitation, and the XPS and EXAFS analysis results suggested that uranium presented as uranyl oxyhydroxide species together with maghemite and magnetite (Scott et al., 2005).

Research studies have also confirmed that magnetite could reduce U(VI) to U(IV). Singer reported that an important pathway for U(VI) reduction was by Fe(II)-bearing minerals, particularly magnetite. Massey reported that heterogeneous uranium reduction by reducing minerals, such as Fe sulfides and magnetite, was also possible because magnetite was formed via homogeneous uranium reduction by Fe(II) or sulfide (Hua et al., 2006; Hua and Deng, 2008; Latta et al., 2012; Hyun et al., 2012; Du et al., 2011). Therefore, uranium in this system was determined to be associated with iron oxide minerals (ferrihydrite, goethite, magnetite, etc.) and uranium minerals (UO_2) (Massey et al., 2014). Ilton reported that the heterogeneous reduction of U(VI) to

U(IV) by ferrous iron was a key process that influenced the transportation and remediation of uranium in the environment and indicated that a strategy for restricting uranium mobility was to reduce it to (and maintain it as) U(IV). The U(VI)-magnetite system received appreciable attention because magnetite is a ubiquitous ferrous-bearing oxide and a corrosion product of steel, and it presents ramifications for the storage of nuclear waste (Ilton et al., 2010). The possible reaction equation between U(VI) and Fe_3O_4 was:



The reaction of UO_2^{2+} and Fe_3O_4 is illustrated in Fig. 6, which explains the reaction model.

The surface reduction of aqueous U(VI) to solid U(IV) occurred by direct electron transfer with structural Fe(II) at the magnetite surface. The majority of surface reduction occurred within 48 hr of exposure to the uranium solution. The experimental results of Latta et al. also suggested that U(IV) could be stabilized on mineral surfaces because of an abiotic reduction by Fe(II) (e.g., U(VI) reduction by Fe_3O_4) and a coupled biotic–abiotic reduction pathway involving an electron shuttle (Latta et al., 2014).

In our samples, the U(VI) in the raw CBA likely reduced to U(IV) accompanied with Fe(II). After magnetic separation, ferrous particles were enriched with magnetite. Therefore, U(IV) was concentrated in the iron-rich particles. However, uranium in the iron-rich fraction accounted for 45% of the total uranium (Sun et al., 2016), which meant that the amount of iron in the CBA was not sufficient to reduce the major U(VI) species to U(IV). Thus, an artificial ferrous solution should be added to reduce uranium.

2.4. Reduction of U(VI) to U(IV) by adding FeSO_4 solution

The above discussion indicates that ferrous solution can reduce U(VI) to U(IV) in CBA. Because U(IV) is insoluble, uranium can be immobilized. To reduce the migration of uranium in the CBA, FeSO_4 solution was added as a reductive reagent to the bottom ash heap. The uranium content in the leachates was determined by an inductively coupled plasma mass spectrometer (ICP-MS) after extracted by TBP, which was stated in Section 1.2. The analyses of uranium leachability indicated that U(VI) was

Table 3 – Linear combination fit applied to XANES spectra.

Sample	UO_2	U_3O_8	$\text{UO}_2(\text{NO}_3)_2$	UO_3	R-factor	χ^2
Raw CBA	0.187	0.718	0.000	0.121	0.000297	0.014
Iron-rich 1	0.914	0.100	0.026	0.000	0.000251	0.013
Iron-rich 2	0.919	0.047	0.077	0.000	0.000509	0.025
Acid leached residue	0.620	0.206	0.221	0.000	0.000891	0.043

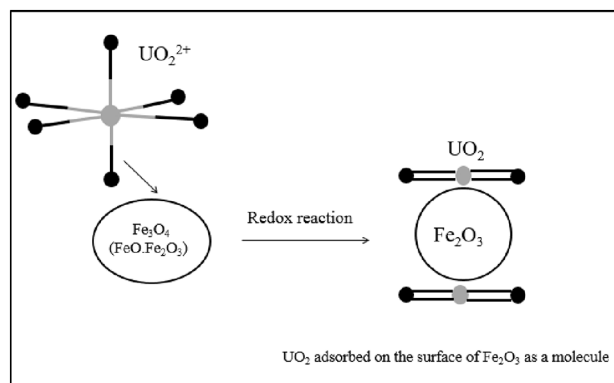


Fig. 6 – Model illustrating changes of uranium at magnetite surfaces by redox reaction.

reduced to U(IV) after several months because only 2.31% of the total uranium was leached out as U(VI). The remaining U in the leached tailings accounted for 96.57% of the total uranium in the CBA. The results indicated that U(VI) was almost completely reduced to U(IV) when infiltrated with the FeSO_4 solution for 6 months. Moreover, under these circumstances, the uranium in the bottom ash heap was immobilized and hardly leached out by the acid rain. Therefore, uranium pollution to the surrounding environment could be prevented or at least alleviated.

2.5. Environmental implications for U immobility in CBA

The above discussion indicated that the uranium in the CBA mainly occurred as U(VI) and migrated with the acid rain leachate. However, after immobilization by the addition of the FeSO_4 solution to the ash heap, a dramatic decrease in U(VI) leaching was observed. Once the surrounding environment is considered, the arable lands surrounding the ash heaps, including the soil and underground water supply, could be protected from uranium pollution. Under current conditions, uranium migration from ash to the surrounding soils, water and plants contaminates the environment, and millions of inhabitants are impacted daily (Lei et al., 2014). Therefore, uranium migration impacts the health of societies, economies and communities. By limiting uranium migration around the CBA heap, radioactive pollution can be alleviated. Overall, immobilizing uranium from CBA is a beneficial technique, and local governments should be willing to provide financial support for such efforts.

Acknowledgments

This work was supported by the Talent Support Fund of Tsinghua University (No. 413405001).

REFERENCES

Allen, P.G., Shuh, D.K., Bucher, J.J., et al., 1996. Determinations of uranium structures by EXAFS: schoepite and other U(VI) oxide precipitates. *Radiochim. Acta* 75 (1), 47–54.

- Bertsch, P.M., Hunter, D.B., Sutton, S.R., Bajt, S., Rivers, M.L., 1994. In situ chemical speciation of uranium in soils and sediments by Micro X-ray absorption spectroscopy. *Environ. Sci. Technol.* 28 (5), 980–984.
- Dodge, C.J., Francis, A.J., Gillow, J.B., Halada, G.P., Clayton, C.R., 2002. Association of uranium with iron oxides typically formed on corroding steel surfaces. *Environ. Sci. Technol.* 36, 3504–3511.
- Dong, W.M., Brooks, S.C., 2006. Determination of the formation constants of ternary complexes of uranyl and carbonate with alkaline earth metals (Mg^{2+} , Ca^{2+} , Sr^{2+} and Ba^{2+}) using anion exchange method. *Environ. Sci. Technol.* 40, 4689–4695.
- Du, X., Boonchayaanant, B., Wu, W.M., Fendorf, S., Bargar, J., Criddle, C.S., 2011. Reduction of uranium(VI) by soluble iron(II) conforms with thermodynamic predictions. *Environ. Sci. Technol.* 45 (11), 4718–4725.
- Flues, M., Camargo, I.M.C., Silva, P.S.C., Mazzilli, B.P., 2006. Radioactivity of coal and ashes from Figueira coal power plant in Brazil. *J. Radioanal. Nucl. Chem.* 270, 597–602.
- Grambow, B., Smailos, E., Geckeis, H., Müller, R., 1996. Sorption and reduction of uranium(VI) on iron corrosion products under reducing saline conditions. *Radiochim. Acta* 74, 149–154.
- Gui, L., Yang, Y.Q., Jeon, S.W., Gillham, R.W., Blowes, D.W., 2009. Reduction of chromate by granular iron in the presence of dissolved CaCO_3 . *Appl. Geochem.* 24, 677–686.
- Henning, C., Reich, T., Dahn, R., Scheidegger, A.M., 2002. Structure of uranium sorption complexes at montmorillonite edge sites. *Radiochim. Acta* 90 (9–11), 653–657.
- Hsiao, M.C., Wang, H.P., Huang, Y.J., Yang, Y.W., 2001. EXAFS study of copper in waste incineration fly ashes. *J. Synchrotron Radiat.* 8, 931–933.
- Hsiao, M.C., Wang, H.P., Chang, J.E., Peng, C.Y., 2006. Tracking of copper species in incineration fly ashes. *J. Hazard. Mater.* 138, 539–542.
- Hua, B., Deng, B., 2008. Reductive immobilization of uranium(VI) by amorphous iron sulfide. *Environ. Sci. Technol.* 42, 8703–8708.
- Hua, B., Xu, H., Terry, J., Deng, B., 2006. Kinetics of uranium(VI) reduction by hydrogen sulfide in anoxic aqueous systems. *Environ. Sci. Technol.* 40 (15), 4666–4671.
- Huggins, F.E., Huffman, G.P., 1996. Modes of occurrence of trace elements in coal from XAFS spectroscopy. *International Journal of Coal Geology* 32 (1–4), 31–53.
- Huggins, F.E., Shah, N., Huffman, G.P., Robertson, J.D., 2000. XAFS spectroscopic characterization of elements in combustion ash and fine particulate matter. *Fuel Process. Technol.* 65–66, 203–218.
- Hyun, S.P., Davis, J.A., Sun, K., Hayes, K.F., 2012. Uranium(VI) reduction by iron(II) monosulfide mackinawite. *Environ. Sci. Technol.* 46, 3369–3376.
- Ilton, E.S., Boily, J.F., Buck, E.C., Skomurski, F.N., Rosso, K.M., Cahill, C.L., et al., 2010. Influence of dynamical conditions on the reduction of U(VI) at the magnetite-solution interface. *Environ. Sci. Technol.* 44 (1), 170–176.
- Langmuir, D., 1978. Uranium solution-mineral equilibria at low temperatures with applications to sedimentary ore-deposits. *Geochim. Cosmochim. Acta* 42, 547–569.
- Latta, D.E., Gorski, C.A., Boyanov, M.I., O’Loughlin, E.J., Kemner, K.M., Scherer, M.M., 2012. Influence of magnetite stoichiometry on U(VI) reduction. *Environ. Sci. Technol.* 46, 778–786.
- Latta, D.E., Mishra, B., Cook, R., Kemner, K.M., Boyanov, M.I., 2014. Stable U(IV) complexes form at high-affinity mineral surface sites. *Environ. Sci. Technol.* 48 (3), 1683–1691.
- Laurette, J., Larue, C., Llorens, I., Jaillard, D., Jouneau, P.H., Bourguignon, J., et al., 2012. Speciation of uranium in plants upon root accumulation and root-to-shoot translocation: A XAS and TEM study. *Environ. Exp. Bot.* 77, 87–95.
- Lei, X.F., Qi, G.X., Sun, Y.L., Xu, H., 2014. Removal of uranium and gross radioactivity from coal bottom ash by CaCl_2 roasting followed by HNO_3 leaching. *J. Hazard. Mater.* 276, 346–352.

- Mansour, A.N., Melendres, C.A., 1998. Analysis of X-ray absorption spectra of some nickel oxycompounds using theoretical standards. *J. Phys. Chem. A* 102, 65–81.
- Massey, M.S., Lezama-Pacheco, J.S., Jones, M.E., Ilton, E.S., Cerrato, J.M., Bargar, J.R., et al., 2014. Competing retention pathways of uranium upon reaction with Fe(II). *Geochim. Cosmochim. Acta* 142, 166–185.
- Mei, H., Tan, X., Yu, S., Ren, X., Chen, C., Wang, X., 2015. Effect of silicate on U(VI) sorption to Al_2O_3 : batch and EXAFS studies. *Chem. Eng. J.* 269, 371–378.
- Mohan, M.S., Zingaro, R.A., Macfarlane, R.D., Irgolic, K.J., 1982. Characterization of a uranium-rich organic material obtained from a South Texas lignite. *Fuel* 61, 853–858.
- Newville, M., 2001. IFEFFIT: interactive XAFS analysis and FEFF fitting. *J. Synchrotron Radiat.* 8, 322–324.
- Papp, Z., Dezsó, Z., Daróczy, S., 2002. Significant radioactive contamination of soil around a coal-fired thermal power plant. *J. Environ. Radioact.* 59, 191–205.
- Scott, B.G., Allen, C., Heard, P.J., Randell, M.G., 2005. Reduction of U(VI) to U(IV) on the surface of magnetite. *Geochim. Cosmochim. Acta* 69 (24), 5639–5646.
- Seredin, V.V., Finkelman, R.B., 2008. Metalliferous coals: a review of the main genetic and geochemical types. *Int. J. Coal Geol.* 76, 253–289.
- Singer, D.M., Chatman, S.M., Ilton, E.S., Rosso, K.M., Banfield, J.F., Waychunas, G.A., 2012. U(VI) sorption and reduction kinetics on the magnetite (111) surface. *Environ. Sci. Technol.* 46, 3821–3830.
- Stewart, B.D., Mayes, M.A., Fendorf, S., 2010. Impact of uranyl-calcium-carbonate complexes on uranium(VI) adsorption to synthetic and natural sediments. *Environ. Sci. Technol.* 44, 928–934.
- Strehle, M., 2011. X-ray photoelectron spectroscopy(XPS) study of single crystal UO_2 and U_3O_8 on R-plane sapphire and yttrium stabilized zirconium(YSZ) substrates. First ed. Master degree thesis, (Illinois).
- Sun, Y.L., Qi, G.X., Lei, X.F., Xu, H., Li, L., Yuan, C., et al., 2016. Distribution and mode of occurrence of uranium in bottom ash derived from high-germanium coals. *J. Environ. Sci.* 43, 91–98.
- Takaoka, M., Yamamoto, T., Shiono, A., Takeda, N., Oshita, K., Matsumoto, T., et al., 2005. The effect of copper speciation on the formation of chlorinated aromatics on real municipal solid waste incinerator fly ash. *Chemosphere* 59, 1497–1505.
- Vanden, B.S., Laval, J.P., Gaudreau, B., Terryn, H., Verwerft, M., 2000. XPS investigations on cesium uranates: mixed valency behaviour of uranium. *J. Nucl. Mater.* 277 (1), 28–36.
- Wang, X.L., Fu, Y.B., Xie, R.S., 1997. The X-ray photoelectron spectroscopy study of triuranium octaoxide. *Nucl. Tech.* 20 (4), 210–214.
- Wu, Z.Y., Ouvrard, G., Gressier, P., Natoli, C.R., 1997. Ti and O K edges for titanium oxides by multiple scattering calculations: comparison to XAS and EELS spectra. *Phys. Rev. B* 55, 10382.
- Wu, Z.Y., Xian, D.C., Natoli, C.R., Marcelli, A., Paris, E., Mottana, A., 2001. Symmetry dependence of X-ray absorption near-edge structure at metal K edge of 3d transition metal compounds. *Appl. Phys. Lett.* 79, 1918.
- Wu, Z.Y., Xian, D.C., Hu, T.D., Xie, Y.N., Tao, Y., Natoli, C.R., et al., 2004. Quadrupolar transitions and medium-range-order effects in metal K-edge X-ray absorption spectra of 3d transition-metal compounds. *Phys. Rev. B* 70, 33104.
- Yang, J., 2007. Concentration and distribution of uranium in Chinese coals. *Energy* 32, 203–212.
- Yang, Z., Liu, L., Chai, L., 2014. Arsenic immobilization in the contaminated soil using poorly crystalline Fe-oxyhydroxy sulfate. *Environ. Sci. Pollut. Res.* 22, 12624–12632.
- Zhang, J., Ouyang, Y., Ling, D., 2007. Impacts of simulated acid rain on cation leaching from the Latosol in south China. *Chemosphere* 67, 2131–2137.
- Zhang, F.X., Lang, M., Wang, J.W., 2014. High-pressure U_3O_8 with the fluorite-type structure. *J. Solid State Chem.* 213, 110–115.